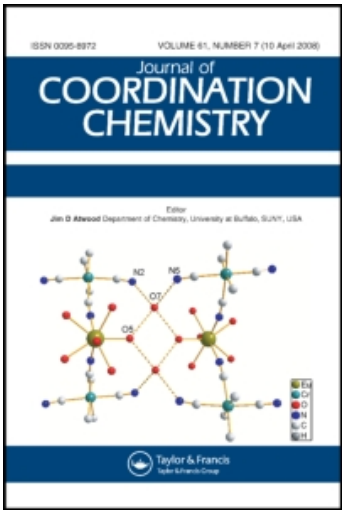

Journal of Coordination Chemistry
Publication details, including instructions for authors and subscription information:
http://www.informaworld.com/smpp/title~content=t713455674

Synthesis, characterization, DNA binding, photo-induced DNA cleavage, and antimicrobial activity of metal complexes of a Schiff base derived from *bis*(3-aminophenyl)malonamide

N. Raman[a]; A. Sakthivel[a]; R. Jeyamurugan[a]
[a] Research Department of Chemistry, VHNSN College, Virudhunagar 626001, India

First published on: 22 September 2010

To cite this Article Raman, N. , Sakthivel, A. and Jeyamurugan, R.(2009) 'Synthesis, characterization, DNA binding, photo-induced DNA cleavage, and antimicrobial activity of metal complexes of a Schiff base derived from *bis*(3-aminophenyl)malonamide', Journal of Coordination Chemistry, 62: 24, 3969 — 3985, First published on: 22 September 2010 (iFirst)
To link to this Article: DOI: 10.1080/00958970903288294
URL: http://dx.doi.org/10.1080/00958970903288294

Journal of Coordination Chemistry
Vol. 62, No. 24, 20 December 2009, 3969–3985

Synthesis, characterization, DNA binding, photo-induced DNA cleavage, and antimicrobial activity of metal complexes of a Schiff base derived from *bis*(3-aminophenyl)malonamide

N. RAMAN*, A. SAKTHIVEL and R. JEYAMURUGAN

Research Department of Chemistry, VHNSN College, Virudhunagar 626001, India

(*Received 28 March 2009; in final form 3 July 2009*)

The peptide linkage Schiff base (H_2L) and its complexes have been synthesized and fully characterized by elemental analysis, UV–Vis, FTIR, ^{1}H-NMR, ^{13}C-NMR, EPR, and FAB-mass spectra. The stoichiometry of the complexes is [ML] (where M = Cu(II), Co(II), Ni(II), Zn(II), and VO(IV)). All the complexes exhibit square-planar geometry except the vanadyl complex which has square-pyramidal geometry. Interactions of the complexes and free ligand with double-stranded calf thymus DNA (CT-DNA) are studied by UV-spectrophotometric, electrochemical, and viscosity measurements. The data suggest that all the complexes form adducts with DNA and distort the double helix by changing the base stacking. Vanadyl complex forms a weaker adduct to CT-DNA than other complexes, probably due to the square-pyramidal geometry. CT-DNA induces extensive distortion in the planarity of vanadyl complex as EPR spectral calculations reveal. The intrinsic binding constants (K_b) of [ZnL], [CuL], [CoL], and [NiL] are 1.1×10^5, 1.4×10^5, 0.8×10^5, and $0.6 \times 10^5\,M^{-1}$, respectively. Photo-induced DNA cleavage indicates that all complexes cleave DNA effectively. Control DNA cleavage experiments using pUC19 supercoiled (SC) DNA and minor groove binder distamycin suggest major groove binding for the synthesized complexes. The antimicrobial results indicate that the complexes inhibit the growth of bacteria and fungi more than the free ligand.

Keywords: Intrinsic binding constant; Photo-induced DNA cleavage; Square-planar geometry; Antimicrobial activity

1. Introduction

Transition metal complexes containing tetraaza Schiff-base ligands have been of interest for many years [1, 2] because of the versatility of their steric and electronic properties. Linear and cyclic Schiff bases obtained by condensation of primary amines with aldehydes, and their associated metal complexes, find a variety of applications including biological, clinical, analytical, and industrial [3].

Different forms of DNA such as A, B, and Z play various biological roles. DNA attains different conformations, particularly when it interacts with various biological macromolecules *in vitro* and/or *in vivo* [4, 5]. These different DNA forms are important in discharging various biological roles of DNA.

*Corresponding author. Email: drn_raman@yahoo.co.in

ISSN 0095-8972 print/ISSN 1029-0389 online
DOI: 10.1080/00958970903288294

Transition metal complexes containing spectroscopically active metal centers can be used as probes of biological systems. The use of poly-pyridine metal complexes as artificial nucleases [6, 7] has been an active area of research, however, has remained largely unexploited in the field of studies of biologically relevant metallo-peptide complexes with DNA. Metallo-peptide complexes play a vital role in the maintenance of physiological redox equilibria [8], signal transduction [9], gene expression [10], and apoptosis [11].

Although the redox behaviors of a number of metal complexes containing Schiff-base ligands have been studied, the electrochemical properties of such complexes are not completely clear [12]. Several researchers have proposed that the redox potential in macrocyclic Schiff-base complexes is directly related to many biologically relevant chemical characteristics of the entire complex, e.g., dioxygen binding, nucleophilicity [13, 14], and DNA binding and cleavage. Thus, there has been strong interest in determining thermodynamically meaningful redox potentials of Schiff-base complexes and in understanding the relationship between these potentials and the interaction of DNA [15].

In this work, we disclose a simple procedure for the synthesis of transition metal Schiff-base complexes containing azomethine and peptide linkage and biological studies such as DNA binding, photo-induced DNA cleavage, and antimicrobial activity.

2. Experimental

2.1. *Materials and methods*

All reagents and chemicals were procured from Merck. Solvents used for electrochemical and spectroscopic studies were purified by standard procedures [16]. DNA was purchased from Bangalore Genei (India). Agarose (molecular biology grade) and ethidium bromide (EB) were obtained from Sigma (USA). *Tris*(hydroxymethyl)-aminomethane hydrochloride (Tris-HCl) buffer solution was prepared using deionized, sonicated triple-distilled water.

Carbon, hydrogen, and nitrogen analyses of the complexes were carried out on a CHN analyzer Carlo Erba 1108, Heraeus. Infrared spectra (4000–400 cm^{-1} KBr discs) of the samples were recorded on a Perkin–Elmer 783 series FTIR spectrophotometer. Electronic absorption spectra from 200 to 1100 nm were obtained on a Shimadzu UV-1601 spectrophotometer. The ^{1}H- and ^{13}C NMR spectra (300 MHz) of the ligand and its zinc complex were recorded on a Bruker Avance DRX 300 FT-NMR spectrometer using $CDCl_3$ and DMSO-d_6 with trimethylsilane as internal standard. Fast atom bombardment mass spectra of the complexes were recorded on a JEOL SX 102/DA-6000 mass spectrometer/data system using Argon/Xenon (6 kV, 10 mA). The accelerating voltage was 10 kV and the spectra were recorded at room temperature using *m*-nitrobenzylalcohol (NBA) as the matrix. X-band ESR spectra of the complexes were recorded at RT (300 K) and LNT (77 K) using tetracyanoethylene (TCNE) as the g-marker. Molar conductances of 10^{-3} M solutions of the complexes in N,N′-dimethylformamide (DMF) were measured at room temperature with a Deepvision Model-601 digital direct reading deluxe conductivity meter. Magnetic susceptibility measurements were carried out by employing the Guoy method at room

temperature on powder sample of the complex using $CuSO_4 \cdot 5H_2O$ as calibrant. The purities of ligand and complexes were evaluated by column and thin layer chromatography.

2.1.1. Estimation of metal. The metals were estimated gravimetrically as their oxides [17] by fusion with AnalaR ammonium oxalate. In a typical experiment, about 0.3 g of the dried complex was accurately weighed in a previously weighed silica crucible. AnalaR ammonium oxalate, roughly three parts by weight of the complex, was added and the mixture was incinerated slowly at first and then strongly using a Bunsen burner for 3 h. It was then cooled in a desiccator and weighed. The procedure was repeated till the final oxide weight was constant. From the weight, the percentage of metal in the complex was calculated.

2.2. *Synthesis*

2.2.1. Synthesis of peptide linkage Schiff base (H_2L). An ethanolic solution of diethylmalonate (1.6 g, 10 mM) was refluxed with an ethanolic solution of *m*-phenylenediamine (2.16 g, 20 mM) for *ca* 3 h in the presence of the catalyst 1,3-dicyclohexylcarbodiimide (DCC) [18]. The solvent was then evaporated until the mixture was almost dry, and the residue was treated with 30 mL of cold water and ethanol. The organic layer was dried over anhydrous Na_2SO_4 and evaporated to obtain yellow solid which was filtered off, washed with ethanol and diethyl ether, and dried *in vacuo*.

An ethanolic (50 mL) solution of the above product (2.84 g, 10 mM) was refluxed with 2-hydroxy-3-methoxybenzaldehyde (2.98 g, 20 mM) taken in ethanol (50 mL) with anhydrous K_2CO_3 (1 g) for about 6 h. Then, the potassium carbonate was filtered from the reaction mixture and the resulting solution was concentrated to 25 mL on a water bath and allowed to cool at room temperature. The solid product formed was separated by filtration and washed thoroughly with ethanol and then dried *in vacuo*. Anal. Calcd for $C_{31}H_{28}N_4O_6$ (%): C, 67.3; H, 5.1; N, 10.1. Found (%): C, 66.9; H, 5.0; N, 9.9. Yield: 61%; FT-IR (KBr disc): 3160 (N–H), 1708 (C=O), 1630 (C=N), 3250–3500 (–OH) cm^{-1}, 2350 (–CH). ^{1}H-NMR ($CDCl_3$): (phenyl multiplet) 6.7–7.2 δ (m); δ(–OCH_3), 3.4 (s); δ (–HN–C=O), 8.9 (s); δ(–N=CH–), 7.8; δ (–CH_2–) 2.3; δ (–OH) 12.4; λ_{max} in EtOH, 46,642; 27,777 cm^{-1} (214.4 and 360 nm). *m*/*z*, 552 (10.5%).

The outline of the synthesis of ligand is given in scheme 1.

2.2.2. Synthesis of metal complexes (ML). A solution of the metal chloride/vanadyl sulfate (5 mM) in absolute ethanol (20 mL) was added to a solution of the ligand (2.765 g, 5 mM) in absolute ethanol (20 mL) and the mixture was refluxed for 3–4 h. At the end of the reaction, determined by thin layer chromatography, the precipitate was filtered off, washed with ethanol and diethyl ether, and dried *in vacuo*. Anal. Calcd for $C_{31}H_{26}N_4O_6Cu$ (%): C, 60.6; H, 4.2; N, 9.1; Cu, 10.3. Found (%): C, 60.4; H, 4.1; N, 8.9; Cu, 10.1. Yield: 53%; FT-IR (KBr disc): 3158 (N–H), 1701 (C=O), 1608 (C=N), 482 (M–O), 430 (M–N) cm^{-1}, 2350 (–CH). λ_M 10^{-3} ($Ohm^{-1}\,cm^2\,mol^{-1}$), 12. μ_{eff} (BM), 1.8, λ_{max} in DMF, 35,714, 29,411, 22,988, and 16,391 cm^{-1} (282.4, 340, 435, and 610 nm), *m*/*z*, 614 (11.2%).

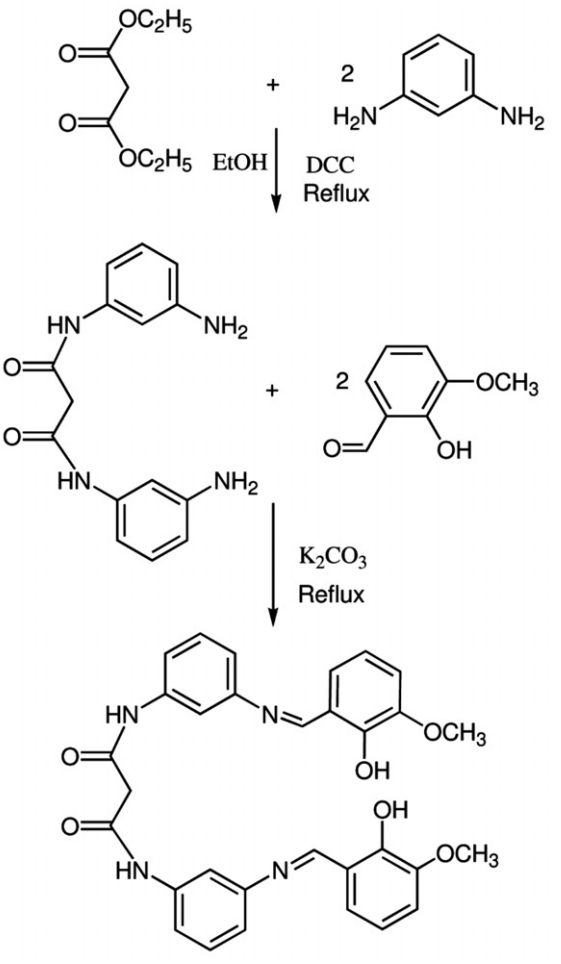

Scheme 1. The outline of the synthesis of ligand (H_2L).

Anal. Calcd for $C_{31}H_{26}N_4O_6Ni$ (%): C, 61.1; H, 4.3; N, 9.2; Ni, 9.6. Found (%): C, 60.9; H, 4.2; N, 9.1; Ni, 9.4. Yield: 42 %; FT-IR (KBr disc): 3162 (N–H), 1701 (C=O), 1602 (C=N), 522 (M–O), 425 (M–N) cm^{-1}. λ_M 10–3 ($ohm^{-1}\,cm^2\,mol^{-1}$), 14. μ_{eff} (BM), diamagnetic. λ_{max} in DMF, 29498, 19417, and 14,184 cm^{-1} (339, 515 and 705 nm), m/z, 609 (15.4%).

Anal. Calcd for $C_{31}H_{26}N_4O_6Co$ (%): C, 61.0; H, 4.3; N, 9.1; Co, 9.6. Found (%): C, 59.7; H, 4.2; N, 9.0; Co, 9.4. Yield: 49%; FT-IR (KBr disc): 3157 (N–H), 1705 (C=O), 1604 (C=N), 494 (M–O), and 444 (M–N) cm^{-1}. λ_M 10^{-3} ($Ohm^{-1}\,cm^2\,mol^{-1}$), 12. μ_{eff} (BM), 4.73. λ_{max} in DMF, 45,045, 29,069, and 15,408 cm^{-1} (222, 344, and 649 nm), m/z, 609 (14.8%).

Anal. Calcd for $C_{31}H_{26}N_4O_6Zn$ (%): C, 60.4; H, 4.2; N, 9.1; Zn, 10.6. Found (%): C, 60.0; H, 4.2; N, 9.0; Zn, 10.4. Yield: 32%; FT-IR (KBr disc): 3160 (N–H), 1702 (C=O), 1605 (C=N), 482 (M–O), and 424 (M–N) cm^{-1}. ^{1}H-NMR (DMSO-d_6): (phenyl multiplet) 6.7–7.2 δ(m); δ(–OCH_3), 3.4 (s); δ(–HN–C=O), 8.6 (s), δ(–N=CH–),

7.6, δ (–CH_2–) 2.2, δ λ_M 10^{-3} ($Ohm^{-1}\,cm^2\,mol^{-1}$), 21. μ_{eff} (BM), diamagneric, m/z, 615 (21.4%).

Anal. Calcd for $C_{31}H_{26}N_4O_7V$ (%): C, 60.3; H, 4.2; N, 9.0; V, 8.2. Found (%): C, 60.0; H, 4.1; N, 8.6; V, 7.9. Yield: 58%; FT-IR (KBr disc): 3157 (N–H), 1707 (C=O), 1620 (C=N), 511 (M-O), 439 (M–N), and 968 (V=O) cm^{-1}. λ_M 10^{-3} ($ohm^{-1}\,cm^2\,mol^{-1}$), 19. μ_{eff} (BM), 1.79. λ_{max} in DMF, 41,152, 29,673, 19,157, and 12,165 cm^{-1} (243, 337, 522, and 822 nm), m/z, 617 (18.7%).

2.3. *DNA binding and cleavage experiments*

All experiments involving the interaction of the complexes with calf thymus DNA (CT-DNA) were carried out in Tris-HCl buffer (50 mM Tris-HCl, pH 7.2) containing 5% DMF at room temperature. A solution of CT-DNA in the buffer gave a ratio of UV absorbance at 260 and 280 nm of about 1.89 : 1, indicating CT-DNA sufficiently free from protein [19]. The CT-DNA concentration per nucleotide was determined by absorption spectroscopy using the molar absorption coefficient of 6600 $M^{-1}\,cm^{-1}$ at 260 nm [20].

2.4. *Absorption spectroscopic studies*

Absorption titration experiments were performed by maintaining the metal complex concentration as constant at 50 μM while varying the concentration of the CT-DNA within 40–400 μM. While measuring the absorption spectra, equal quantity of CT-DNA was added to both the complex solution and the reference solution to eliminate the absorbance of CT-DNA itself. From the absorption data, the intrinsic binding constant (Kb) was determined from a plot of [DNA]/($\varepsilon_a - \varepsilon_f$) *versus* [DNA] using equation (1):

$$[DNA]/(\varepsilon_a - \varepsilon_f) = [DNA]/(\varepsilon_b - \varepsilon_f) + [K_b(\varepsilon_b - \varepsilon_f)]^{-1} \quad (1)$$

where [DNA] is the concentration of CT-DNA in base pairs. The apparent absorption coefficients ε_a, ε_f, and ε_b correspond to A_{obsd}/[M], the extinction coefficient for the free metal(II) complex and extinction coefficient for the metal(II) complex in the fully bound form, respectively [21]. K_b is given by the ratio of slope to intercept.

2.5. *Electrochemical methods*

Cyclic and differential pulse voltammetry were performed on a CHI 620C electrochemical analyzer with three electrode system: gold as working electrode, platinum wire as auxiliary electrode, and Ag/AgCl as reference electrode. Solutions were deoxygenated by purging with N_2 prior to measurements. The freshly polished gold electrode was modified by transferring a droplet of 2 μL of 3×10^{-3} M CT-DNA solution onto the surface, followed by air drying. Then the electrode was rinsed with distilled water. Thus, a CT-DNA-modified gold electrode was obtained [22].

2.6. *Viscosity measurements*

Viscosity experiments were carried out on an Ostwald viscometer, immersed in a thermostated water-bath maintained at 30.0°C ± 0.1°C. CT-DNA samples of approximately 0.5 mM were prepared by sonicating in order to minimize complexities arising from CT-DNA flexibility [23]. Flow time was measured with a digital stopwatch three times for each sample and an average flow time was calculated. Data are presented as $(\eta/\eta^{o})1/3$ *versus* the concentration of the metal(II) complexes, where η is the viscosity of CT-DNA solution in the presence of complex and η^{o} is the viscosity of CT-DNA solution in the absence of complex. Viscosity values were calculated after correcting the flow time of buffer alone (t_o), $\eta = (t - t_o)/t_o$ [24].

2.7. *DNA cleavage*

The extent of cleavage of super coiled (SC) pUC19 DNA (33.3 μM, 0.2 μg) to its nicked circular (NC) form was determined by agarose gel electrophoresis in 50 mM Tris-HCl buffer (pH 7.2) containing 50 mM NaCl. For photo-induced DNA cleavage studies, the reactions were carried out using UV sources at 360 nm. After exposure to light, each sample was incubated for 1 h at 37°C and analyzed for photo-cleaved products using gel electrophoresis as discussed below [25]. The inhibition reactions for the "chemical nuclease" reactions were carried out in the dark by adding reagents (distamycin 50 μM; DMSO 4 μL) prior to addition of each complex and the reducing agent 3-mercaptopropionic acid (3-MPA). The photo-induced inhibition reactions were carried out at 360 nm using reagents (NaN_3 100 μM; DMSO 4 μL) prior to addition of each complex. For the D_2O experiment, this solvent was used for dilution of the sample to 18 μL, the samples after incubation for 1 h at 37°C in a dark chamber were added to the loading buffer containing 25% bromophenol blue, 0.25% xylene cyanol, 30% glycerol (3 μL), and the solution was finally loaded on 0.8% agarose gel containing 1 μg mL^{-1} ethidium bromide. Electrophoresis was carried out in a dark chamber for 3 h at 50 V in Tris-acetate-EDTA buffer. Bands were visualized by UV light and photographed.

2.8. *Antimicrobial activity*

The *in vitro* biological effects were tested against the bacteria *Salmonella typhi*, *Staphylococcus aureus*, *Escherichia coli*, and *Bacillus subtilis* by the disc diffusion method using agar nutrient as the medium and streptomycin as the standard. Antifungal activities of the compounds were evaluated by the disc diffusion method against *Aspergillus niger*, *Aspergillus flavus*, *Candida albicans,* and *Rhizoctonia bataicola* cultured on potato dextrose agar as medium and nystatin as the standard. The stock solution (0.01–0.005 M) was prepared by dissolving the compounds in DMSO and the solutions were serially diluted in order to find the minimum inhibitory concentration (MIC) values. In a typical procedure [26], the disc was filled with the test solution using a micropipette and the plate was incubated, 24 h for bacteria and 72 h for fungi at 35°C. During this period, the test solution diffused and growth of the inoculated microorganisms was affected.

3. Results and discussion

3.1. *Synthesis and general aspects*

The Schiff base and its Cu(II), Co(II), Ni(II), VO(IV), and Zn(II) complexes have been synthesized and characterized by spectral and analytical data. These data are summarized and given in Section 2. They are air stable with the ligand soluble in common organic solvents, but the complexes are soluble only in DMF and DMSO. The elemental analyses for the metal complexes agree well with the calculated values showing that the complexes have 1 : 1 metal/ligand ratio. The low molar conductances of the complexes in DMF for 10^{-3} M solutions at room temperature are consistent with non-electrolytes with no counter ions (chloride/sulfate) in the complexes. The absence of chloride is evident from Volhard's test and sulfate by $BaCl_2$ test.

3.2. *Mass spectra*

The FAB-mass spectra of ligand and complexes show molecular ion peaks confirming the proposed formula. The mass spectrum of ligand shows the M+ molecular ion peak at m/z 552 (10.5%) corresponding to $[C_{31}H_{28}N_4O_6]^+$. The copper complex molecular ion peak at m/z 614 (11.2%) confirms its stoichiometry as [CuL]. The molecular ion peaks of the Ni(II), Co(II), Zn(II), and VO(IV) complexes were observed at m/z 609 (15.4%), 609 (14.8%), 615 (21.4%), and 617 (18.7%), respectively. Thus, the mass spectral results along with elemental analyses agree with formation of ML complexes of 1 : 1 stoichiometry.

3.3. *IR spectra*

The coordinating atoms were determined from IR spectra of the ligand and complexes. The Schiff base shows characteristic bands for ν(N–H) at 3160 cm^{-1}, ν(C=O) at 1708 cm^{-1}, and ν(C=N) at 1630 cm^{-1} [27] and a broad band at 3250–3500 cm^{-1} due to ν(O–H) of the phenolic hydroxyl which disappears in spectra of the complexes, indicating coordination through deprotonated OH [28]. The ring vibration and C–O stretching modes of the ligand appear at 1476 and 1152 cm^{-1}. In spectra of the complexes these bands are shifted to higher or lower wave number as a result of coordination through the hydroxyl. The ν(M–O) is at 480–525 cm^{-1}. In all the complexes, ν(C=N) bands are shifted by 30–20 cm^{-1} to lower frequencies due to coordination of the azomethine [27]; ν(C=O) and ν(N–H) were not affected in the complexes, indicating that carbonyl and ν(N–H) are not coordinated to the metal ion. Coordination of nitrogen is supported by new bands at 480–525 and 425–450 cm^{-1} assignable to ν(M–O) and ν(M–N) [29]. Accordingly, the ligand is tetradentate through two phenonlic oxygens and two azomethine nitrogens. In addition to other bands, the vanadyl complex shows a band at 940 cm^{-1} from V=O.

3.4. *NMR spectra*

The ^{1}H-NMR spectra of ligand and its zinc complex were recorded in $CDCl_3$ and DMSO-d_6, respectively. The ligand shows phenyl as a multiplet at 6.6–7.2 δ, –OCH_3

at 3.4 δ, –CO–NH at 8.9 δ, –CO–CH_2–CO– at 2.3 δ, and –CH=N– at 7.8 δ. The peak at 12.4 δ attributable to the phenolic –OH is absent in the zinc complex indicating deprotonation of the phenolic –OH on chelation. The azomethine (–N=CH) proton signal in the zinc complex shifts downfield compared to the free ligand, suggesting deshielding of the azomethine due to coordination with metal. There is no appreciable change in all of the other signals of the complex.

The decoupled ^{13}C NMR spectra of macrocyclic ligand (in $CDCl_3$) and its zinc complex (in DMSO-d_6) confirm the presence of azomethine (–C=N–) and peptide (O=C–NH–). In the zinc complex the imine carbon is deshielded compared to free ligand suggesting coordination of azomethine nitrogen to metal ion. Comparison of all other macrocyclic carbon peaks of the ligand with those of the zinc complex [ZnL] shows some up-field and down-field shifts which are not much significant. The data for the free ligand and its zinc complex (Supplementary material) are in good agreement with the assigned structure of the ligand and its complexes.

3.5. *Electronic absorption spectra and magnetic measurements*

The absorption spectrum of L in ethanol exhibits bands at 44,642, 39,062, and 27,777 cm^{-1} (214.4, 256, and 360 nm), attributed to π–π^* and n–π^* transitions. The absorption spectrum of the copper(II) complex in DMF reveals characteristic bands of MLCT transitions at 22,988 and 35,714 cm^{-1} (435 and 282.4 nm) and a strong absorption at 16,391 cm^{-1} (610 nm) assigned to d–d transition characteristic of square-planar d^9 copper involving ($d_{xz}, d_{yz} \rightarrow d_{x^2-y^2}$) orbitals [30]. Magnetic susceptibility in the solid state shows the copper complex to be paramagnetic at ambient temperature with magnetic moment of 1.8 BM within the range normally found for square-planar geometry of other copper complexes.

The nickel complex is diamagnetic and exhibits a strong absorption band in the visible region at 14,184 cm^{-1} (705 nm) $^3A_{2g} \rightarrow {}^3T_{1g}$ and a second more intense band at 19,417 cm^{-1} (515 nm) $^3A_{2g} \rightarrow {}^3T_{1g}$. The square-planar complexes of nickel can readily be distinguished from octahedral or tetrahedral derivatives in that no electronic transition occurs below 10,000 cm^{-1} [31] as a consequence of the large crystal field splitting. This band does not appear which indicates square-planar geometry. The electronic absorption spectrum of cobalt complex gives only one d–d band at 15,408 cm^{-1} (649 nm) corresponding to $^1A_{1g} \rightarrow {}^1B_{1g}$; other bands at 29,069 and 45,045 cm^{-1} (344 and 222 nm) are characteristic of square planar ligand field around Co(II) and can be assigned to $\pi \rightarrow \pi^*$ and $n \rightarrow \pi^*$ charge transfer transitions. The electronic spectrum of oxovanadium complex has bands at 12,165 and 19,157 cm^{-1} (822 and 522 nm), assigned to $^2B_2 \rightarrow {}^2E$ and $^2B_2 \rightarrow {}^2A_1$ transitions, respectively. The geometry of this five coordinated mononuclear complex is a trigonal bipyramid distorted toward a tetragonal pyramid or square-pyramid [32].

3.6. *EPR spectra*

The X-band EPR spectrum of polycrystalline copper complex in DMSO at room temperature exhibits absorption with axial symmetry and partial resolution of hyperfine structure. In DMSO frozen solution, the hyperfine structure is well resolved with four

Table 1. The spin Hamiltonian parameters of Cu(II) and VO(IV) complexes in DMSO at 300 and 77 K.

	Hyperfine constant $\times 10^{-4}\,cm^{-1}$								
Complexes	$A_\parallel$	$A_\perp$	A_{iso}	$g_\parallel$	$g_\perp$	g_{iso}	α^2	β^2	γ^2
[CuL]	167	52	79	2.27	2.07	2.1	0.77	0.86	0.87
[VOL]	167	67	92	1.98	2.04	1.96	0.30	0.92	0.50

lines in the $g_\parallel$ region assigned to interaction of the paramagnetic electron with Cu(II) ($I = 3/2$).

The values obtained for g factor and hyperfine splitting constants A are summarized in table 1. The spectrum shows axial character with $A_\parallel = A_{zz} \gg A_\perp = A_{xx} = A_{yy}$ and $g_{zz} = g_\parallel \gg g_\perp = g_{xx} = g_{yy} > 2.0023$, typical of tetradentate coordination of copper(II). The unpaired electron occupies the $d_{x^2-y^2}$ orbital, having $^2B_{1g}$ as a ground state term [33]. The observed value for the exchange interaction parameter for the copper complex ($G = 4.33$) suggests a weak field, and the local tetragonal axes are aligned parallel or slightly misaligned [34]; exchange coupling effects are not operative in the present copper complex. The value of $g_\parallel/A_\parallel$ is 137 cm^{-1} for copper complex, typical of a slight tetrahedral distortion around Cu(II) in the reduced Schiff base while the Schiff base shows a typical square-plane [35].

The values of $g_\parallel < 2.3$ suggest covalent nature for these complexes with copper–nitrogen and copper–oxygen bonds. To understand the nature of metal–ligand bonding in these complexes, various bonding parameters have been evaluated from the low temperature EPR spectra (table 1).

In-plane σ- and π-bonding are linked to the α and β parameters, respectively, and γ values are representative of out-of-plane π-bonding. The magnitudes of $\alpha^2\beta^2$ and $\alpha^2\gamma^2$ products determine the combined σ- and π-covalent bonding effects with values between 1.0 (100% ionic) and 0.25 (100% covalent) [36]. The values for our copper complex show high in-plane and low out-of-plane π-bonding.

For copper(II) complex with $^2B_{1g}$ ground state ($g_\parallel > g_\perp$), the g values may be expressed as

$$K_\parallel^2 = g[(g_\parallel - 2.0023)\Delta E]/8\lambda_o \tag{2}$$

$$K_\perp^2 = [(g_\perp - 2.0023)\Delta E]/2\lambda_o \tag{3}$$

where λ_o is the spin orbit coupling constant for copper(II) ($-828\,cm^{-1}$), $K_\parallel$ and $K_\perp$ are the parallel and perpendicular components of the orbital reduction factor (K). In case of pure σ-bonding $K_\parallel = K_\perp$, whereas $K_\parallel < K_\perp$ implies considerable in-plane π-bonding, while for out-of-plane π-bonding $K_\parallel > K_\perp$. The calculated values for our complex are close to those reported for similar compounds; the order $K_\parallel > K_\perp$ is typical of covalent and strong out-of-plane π-bonding [37].

The EPR spectra of the vanadyl complex recorded in DMSO at 300 and 77 K show typical 8 and 16 line patterns, respectively. Parameters calculated from the spectra are given in table 1. The observed order $A_\parallel > A_\perp$ and $g_\perp > g_\parallel$ indicates that the unpaired electron is present in the d_{xy} orbital with square-pyramidal geometry around the oxovanadium(IV) chelate [38].

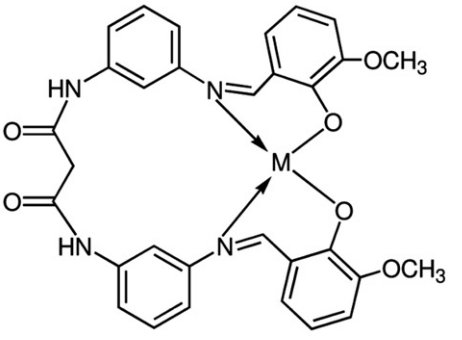

Figure 1. The proposed structure of the Schiff-base complexes. M = Cu((II), Co(II), Ni(II), Zn(II), and VO(IV).

The molecular orbital coefficients α^2 and β^2 were calculated by the following equations [39].

$$\alpha^2 = (2.0023 - g_{\parallel})E/8\lambda\beta^2 \quad (4)$$

$$\beta^2 = 7/6\left(A_{\parallel}/p + A_{\perp}/p + g_{\parallel} - 5/14g_{\perp}9/14g_e\right) \quad (5)$$

$$\gamma^2 = (2.0023 - g_{\perp})E/2\lambda\alpha^2 \quad (6)$$

where $p = 128 \times 10^{-4}\,\mathrm{cm}^{-1}$, $\lambda = 135\,\mathrm{cm}^{-1}$, and E is the electronic transition energy of $^2B_2 \rightarrow {}^2E$. The lower values of α^2 compared to β^2 indicate in-plane π-bonding is more covalent than in-plane σ-bonding.

Based on the above spectral and analytical data, the structure of the Schiff base complexes is given in figure 1.

3.7. *DNA-binding experiments*

3.7.1. Absorption spectroscopic studies. With increasing CT-DNA concentration for the copper complex, hypochromism in the band at 340 nm reaches as high as 27% with a red shift of 3 nm at a ratio of [DNA]/[Cu] of 10. The zinc complex band at 342.6 nm shows hypochromism by about 23% and a red shift of 2.1 nm under the same experimental conditions. These spectral characteristics suggest that these two complexes interact with DNA most likely through a stacking interaction between the aromatic chromophore and the base pairs of DNA. After intercalating the base pairs of DNA, the π^* orbital of the intercalated ligand can couple with the π orbital of the base pairs, thus decreasing the π–π^* transition energy and resulting in bathochromism. The intrinsic binding constant K_b is obtained from the ratio of slope to the intercept from the plots of [DNA]/($\varepsilon_a - \varepsilon_f$) *versus* [DNA]. The K_b values are shown in table 2. Comparing the intrinsic binding constant of the synthesized complexes with those of DNA-intercalatives [40], we can deduce that all the synthesized complexes except vanadyl complex bind strongly to DNA by intercalation; the vanadyl complex forms a weaker adduct to CT-DNA probably due to the square pyramidal geometry of the vanadyl complex.

Table 2. Absorption spectral properties of synthesized complexes with DNA.

	λ_{max}				
Complexes	Free	Bound	$\Delta\lambda$ (nm)	Hypochromicity (%)	$K_b \times 10^5$ (M^{-1})
[CoL]	344.0	342.4	1.6	21.61	0.8
[NiL]	339.0	337.2	1.8	19.45	0.6
[CuL]	340.0	337.0	3.0	27.25	1.4
[ZnL]	342.6	340.5	2.1	23.38	1.1

Table 3. Electrochemical parameters for the interaction of DNA with synthesized complexes.

		E_{pc} (V)		I_{pc} (μA)		$E_{1/2}$ (V)		ΔE_p (V)			
Complex	Redox couple	Free	Bound	Free	Bound	Free	Bound	Free	Bound	k_{red}/k_{oxd}	I_{pc}/I_{pa}
[CoL]	Co(III)/Co(II)	0.302	0.275	0.59	0.38	0.307	0.281	0.283	0.296	0.4	0.74
	Co(II)/Co(I)	−0.092	−0.111	0.36	0.28	–	–	–	–	–	–
	Co(I)/Co(0)	−0.408	−0.418	0.39	0.46	–	–	–	–	–	–
[NiL]	Ni(II)/Ni(I)	−0.327	−0.311	0.73	0.64	–	–	–	–	0.1	–
	Ni(I)/Ni(0)	0.475	0.497	0.20	0.12	–	–	–	–	–	–
[CuL]	Cu(II)/Cu(I)	−0.235	−0.278	0.15	0.08	−0.733	−0.749	0.225	0.257	0.9	0.92
[ZnL]	Zn(II)/Zn(0)	−1.24	−1.46	0.62	0.38	–	–	–	–	<0.1	–

3.7.2. Electrochemical studies. Cyclic and differential pulse voltammetry (Supplementary material) are useful in probing the nature and mode of DNA binding of metal complexes.

In the absence of CT-DNA, the redox couple cathodic peak appears at 0.302 V for Co(III) → Co(II) ($E_{pa} = 0.593$ V, $E_{pc} = 0.302$ V, $\Delta Ep = 0.291$ V, and $E_{1/2} = 0.448$ V) and second redox couple cathodic peak appears at −0.092 V for Co(II) → Co(I) ($E_{pa} = 0.209$ V, $E_{pc} = -0.092$ V, $\Delta Ep = 0.301$ V, and $E_{1/2} = 0.059$ V). The ratio of I_{pc}/I_{pa} is less than unity, indicating that the reaction on gold electrode surface is a quasi-reversible redox process. The incremental addition of CT-DNA to the complex causes a negative shift in $E_{1/2}$ of 16 mV and a decrease in ΔEp of 13 mV. The I_{pc}/I_{pa} values also decrease in the presence of DNA. The decrease of the anodic and cathodic peak currents of the complex in the presence of DNA is due to decrease in the apparent diffusion coefficient of the cobalt(III) complex upon complexation with the DNA macromolecule. The second redox couple of cobalt(II) complex shows no significant change of potential or intensity of current, indicating that the second redox couple species does not stabilize duplex DNA.

In the absence of CT-DNA, only one redox cathodic peak appears at −0.251 V for Cu(II) → Cu(I) ($E_{pa} = 0.482$ V, $E_{pc} = -0.251$ V, $\Delta Ep = 0.733$ V, and $E_{1/2} = 0.116$ V). The redox couple ratio of I_{pc}/I_{pa} is approximately unity, indicating a quasi-reversible redox process. The incremental addition of CT-DNA to the complex causes a negative shift in $E_{1/2}$ and a decrease in ΔEp (table 3). The I_{pc}/I_{pa} values also decrease in the presence of DNA. The decrease of the anodic and cathodic peak currents in the

presence of DNA is due to decrease in the apparent diffusion coefficient upon complexation with the DNA macromolecule showing that copper(II) complex stabilizes the duplex (GC pairs) by intercalation.

In the absence of CT-DNA, the nickel complex shows two cathodic peaks and no anodic peaks. The first cathodic peak appears at −0.327 V for Ni(II) → Ni(I) and second cathodic peak appears at 0.497 V for Ni(I) → Ni(0). Incremental addition of DNA on Ni(II) complex shows a decrease in the current intensity and negative shift of the oxidation peak potential consistent with interaction between Ni(II) and DNA. Zinc(II) complex, oxidation peak at −1.24 V (*Ep*), shows similar behavior.

Electrochemical parameters of the Co(II), Ni(II), Cu(II), and Zn(II) complexes, table 3, show interaction with DNA through intercalation.

Differential pulse voltammograms of the nickel and cobalt complexes in the absence and presence of varying amounts of [DNA] are given in figure 2 and Supplementary material. The increase in concentration of DNA causes a negative potential shift along with the significant decrease of current intensity. The shift in potential is related to the ratio of binding constant:

$$E^{o}_{b'} - E^{o}_{f'} = 0.0591 \log\left(K_{[red]}/K_{[oxd]}\right) \tag{7}$$

where $E^{o}_{b'}$ and $E^{o}_{f'}$ are formal potentials of the Co(III)/Co(II) or Ni(II)/Ni(I) or Cu(II)/Cu(I) complex couple in the bound and free form, respectively. The ratio of the binding

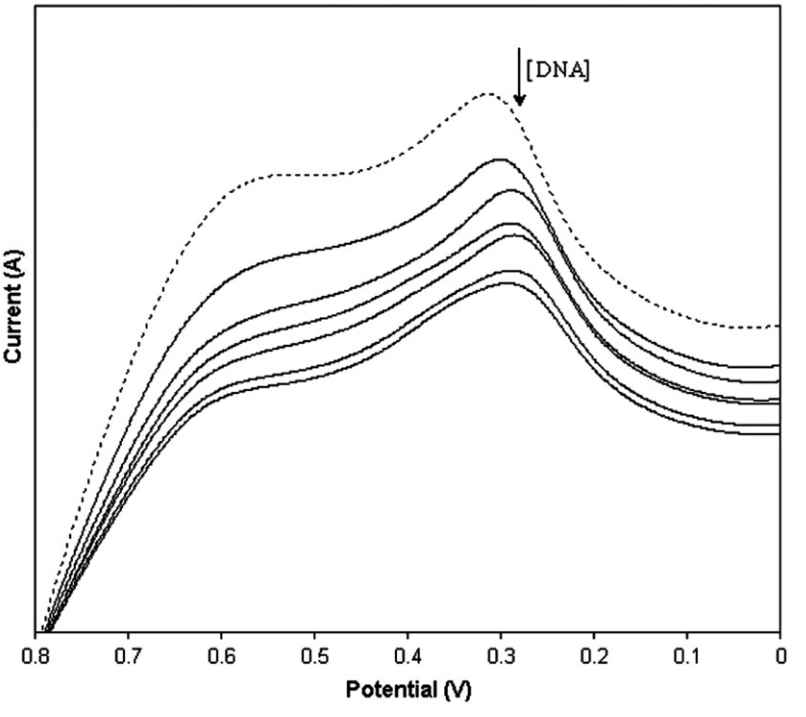

Figure 2. Differential pulse voltammogram of [CoL] in the absence and presence of different concentrations of DNA.

constants ($K_{[red]}/K_{[oxd]}$) for DNA binding were less than unity, indicating preferential stabilization of Co(III), Ni(II), and Cu(II) forms over other forms on binding to DNA.

Differential pulse voltammogram of the Zn(II) complex shows a negative potential shift along with significant decrease of current intensity during addition of increasing amounts of DNA consistent with stabilization of the duplex (GC pairs) by intercalating. Hence, for the complex of the electroactive species (Zn(II)) with DNA, the electrochemical reduction reaction can be divided into two steps:

$$Zn^{2+} - DNA \rightleftharpoons Zn^{2+} + DNA$$
$$Zn^{2+} + 2e^- \rightleftharpoons Zn^0$$

The dissociation constant (K_d) of the Zn(II)–DNA complex was obtained using the following equation:

$$i_p^2 = \frac{K_d}{[DNA]}\left(i_{p^o}^2 - i_p^2\right) + i_{p^o}^2 - [DNA] \quad (8)$$

where K_d is dissociation constant of the complex Zn(II)–DNA, $i_{p^o}^2$, and i_p^2 are reduction current of Zn(II) in the absence and presence of DNA, respectively. Using equation (8), the dissociation constant was determined.

3.7.3. Viscosity measurements. The interaction between the complexes and DNA was investigated by viscosity measurements. Optical photophysical probes provided necessary, but not sufficient clues to support a binding model. Hydrodynamic measurements that were sensitive to length change (i.e., viscosity and sedimentation) are the least ambiguous and most critical tests of binding mode in solution in the absence of crystallographic structural data [41]. A classical intercalation model usually resulted in lengthening the DNA helix, as base pairs were separated to accommodate the binding ligand leading to increase of DNA viscosity. As seen in figure 3, the viscosity of CT-DNA increased with increasing ratio of complexes to CT-DNA, further suggesting an intercalative binding of the complexes with CT-DNA.

3.8. *Chemical nuclease activity of complexes mechanistic investigations*

3.8.1. Oxidative cleavage of DNA. Chemical nuclease activity is controlled by relaxation of supercoiled circular conformation of pUC19 DNA to nicked circular and/or linear conformations. When electrophoresis is applied to circular plasmid DNA, fastest migration will be observed for DNA of closed circular conformations (Form I). If one strand is cleaved, the supercoiled will relax to produce a slower-moving nicked conformation (Form II). If both strands are cleaved, a linear conformation (Form III) will be generated that migrates in between [42].

DNA cleavage by ligand does not occur, indicating the importance of the metal for observing nuclease activity. The oxidative cleavage of pUC19 DNA in the presence of an external reducing agent like 3-MPA (5 mM) has been studied by gel electrophoresis using SC pUC19 DNA (0.2 μg, 33.3 μM) in 50 mM Tris-HCl 50 mM NaCl buffer (14 μL, pH 7.2) and the complexes (50 μM). Control experiments using MPA or the synthesized complexes alone show cleavage of SC DNA under dark

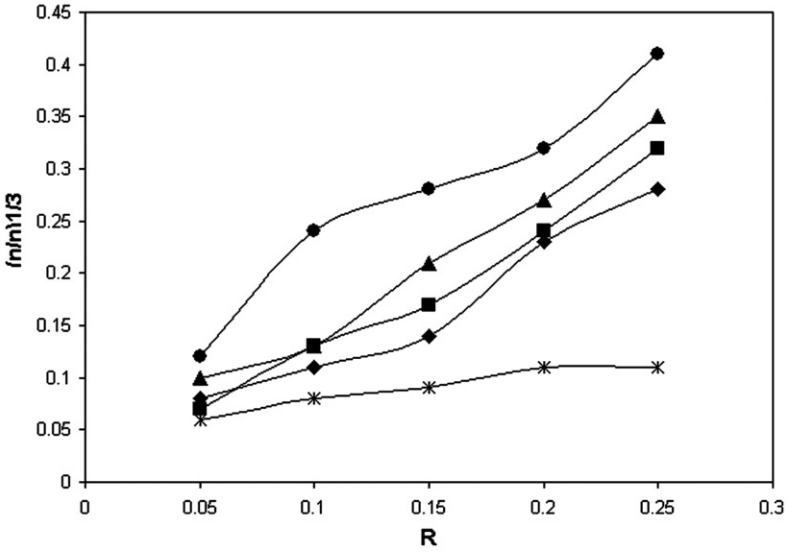

Figure 3. The effect of [VOL] (∗), [ZnL] (•), [CoL] (◆), [NiL] (■), and [CuL] (▲) on the viscosity of DNA; Relative specific viscosity Vs R = [ML]/ [DNA].

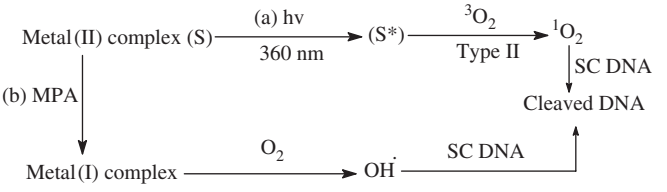

Scheme 2. Mechanistic pathways proposed for (a) photo cleavage reaction (b) for the chemical nuclease activity.

conditions (mechanism (b) in scheme 2), suggesting that the synthesized complexes bind to DNA. To determine the groove selectivity of the complexes, control experiments with minor groove binder distamycin do not inhibit the cleavage for the complexes. This indicates major groove binding for the synthesized complexes with DNA. Control experiments show that the hydroxyl radical scavenger DMSO inhibits DNA cleavage, suggesting the possibility of hydroxyl radical and/or "copper-oxo" intermediate as the reactive species [43]. Superoxide dismutase (SOD) addition does not have any apparent effect on the cleavage activity, indicating non-involvement of superoxide radical in cleavage.

3.8.2. DNA photo-cleavage study. Photo-induced DNA cleavage experiments have been carried out in UV and visible light using the ligand and complexes (50 and 100 μM) and SC pUC19 DNA (0.2 μg, 33.3 μM) in the presence and absence of various inhibitors. The ligand is inactive for DNA cleavage. All the complexes cleave pUC19 DNA from its SC to NC form even in the absence of inhibitors on irradiation with

Table 4. Minimum inhibition concentration of the synthesized compounds against the growth of four fungi ($mg\,mL^{-1}$).

Compound	*A. niger*	*A. flavus*	*C. albicans*	*R. bataicola*
H_2L	78	69	63	71
[CuL]	41	45	53	37
[VOL]	23	27	25	30
[NiL]	38	43	45	37
[CoL]	27	33	50	45
[ZnL]	35	32	41	49
Nystatin	10	8	12	14

Table 5. Minimum inhibition concentration of the synthesized compounds against the growth of four bacteria ($mg\,mL^{-1}$).

Compound	*E. coli*	*S. typhi*	*S. aureus*	*B. subtilis*
H_2L	60	71	74	82
[CuL]	25	27	32	45
[VOL]	20	24	27	20
[NiL]	27	31	38	27
[CoL]	34	29	24	38
[ZnL]	32	24	52	31
Streptomycin	14	18	12	10

UV light at 360 nm. A singlet oxygen quencher like sodium azide inhibits the cleavage. An enhancement of photo-cleavage of DNA is observed in D_2O in which $^1O_2$ has longer lifetime [44]. Hydroxyl radical scavenger DMSO or KI do not show significant inhibition in DNA cleavage. The results indicate a type-II process in which the photo-excited complexes activate molecular oxygen from its stable triplet to cytotoxic singlet state. The proposed mechanistic pathway for photo-induced cleavage of SC-DNA by complex is shown scheme 2.

3.9. *Antimicrobial activity*

The compounds were dissolved in DMSO and soaked in filter paper disc 5 mm diameter and 1 mm thickness. The concentration used in this study ranges from 0.01 to 0.005 M. The discs were placed on previously seeded plates and incubated at 37°C. Streptomycin and nystatin were used as standards for bacteria and fungi, respectively. The MIC values of the investigated compounds are summarized in tables 4 and 5. The complexes exhibit higher antimicrobial activity than the free ligand [45] with [VOL] most potent. Increased activity of the complexes can be explained on the basis of Overtone's [46] and Tweedys chelation theory [47].

4. Conclusion

Macrocyclic tetraaza ligand and its Co(II), Ni(II), Cu(II), and Zn(II) complexes were synthesized and characterized with square-planar geometry around the central

metal ion. Electronic absorption, electrochemical, and viscosity measurement suggest that the complexes bind with DNA through intercalative mode. The gel electrophoresis indicates that they exhibit chemical nuclease activity in the presence of 3-MPA *via* mechanistic pathway involving formation of hydroxyl radical as the reactive species and photo-induced DNA cleavage activity from formation of singlet oxygen ($^1O_2$) as the reactive species in type (II) process. The antimicrobial activity study indicates that the complexes have higher antimicrobial activity than the ligand.

Acknowledgments

The authors express their heartfelt thanks to the College Managing Board, VHNSN College, Virudhunagar, for providing research facilities. N. Raman and A. Sakthivel express their gratitude to the UGC, New Delhi, for financial assistance.

References

[1] Z. Hayvali, D. Yardimci. *Transition Met. Chem.*, **33**, 421 (2008).
[2] B . De Clereq, F. Verpoort. *Macromolecules*, **35**, 8943 (2002).
[3] X.M. Ouyang, B.L. Fei, T.A. Okamura, W.Y. Sun, W.X. Tang, N. Ueyama. *Chem. Lett.*, **31**, 362 (2002).
[4] L. Mefail-Isom, X. Shuiand, L.D. Williams. *Biochemistry*, **37**, 17105 (1998).
[5] C.V. Miduturu, S.K. Silverman. *Angew. Chem. Ed.*, **45**, 1918 (2006).
[6] Y. Prashanthi, K. Kiranmai, N.J.P. Subhashini, P. Shivaraj. *Spectrochim. Acta, Part A*, **70**, 30 (2008).
[7] K.E. Erkkila, D.T. Odom, J.K. Barton. *Chem. Rev.*, **99**, 2777 (1999).
[8] D. Shen, T.P. Dalton, D.W. Nebert, H.G. Shertzer. *J. Biol. Chem.*, **280**, 25305 (2005).
[9] A.P. Arrigo. *Free Radic. Biol. Med.*, **27**, 936 (1999).
[10] C.K. Sen, H. Sies, P.A. Baeuerle. *Antioxidant and Redox Regulation of Genes*, Academic Press, San Diego (1999).
[11] C. Tormos, F. Chaves, M.F. Garcia, F. Garrido, R. Jover, J.E. O'Connor, A. Oliva, G.T. Saez. *Cancer Lett.*, **208**, 103 (2004).
[12] V.T. Kasumov. *Spectrochim. Acta A*, **57**, 2337 (2001).
[13] G. Karthikeyan, P. Pitchaimani. *Transition Met. Chem.*, **28**, 482 (2003).
[14] V.T. Kasumov. *Transition Met. Chem.*, **27**, 228 (2002).
[15] D.F. Averill, R.F. Bromann. *Inorg. Chem.*, **17**, 3389 (1978).
[16] D.D. Perrin, W.L.F. Armarego, D.R. Perrin. *Purification of Laboratory Chemicals*, Pergamon Press, Oxford (1980).
[17] R.J. Angelici. *Synthesis and Techniques in Inorganic Chemistry*, W.B. Saunders Company, Philadelphia (1969).
[18] B.E. Maryanoff, M.N. Greco, H. Zhang, P. Andrade-Gordon, J.A. Kauffman, K.C. Nicolau, A. Liu, P.H. Brungs. *J. Am. Chem. Soc.*, **117**, 1225 (1995).
[19] J. Marmur. *J. Mol. Biol.*, **3**, 208 (1961).
[20] M.E. Reichmann, S.A. Rice, C.A. Thomas, P. Doty. *J. Am. Chem. Soc.*, **76**, 3047 (1954).
[21] A. Wolfe, G.H. Shimer, T. Meehan. *Biochemistry*, **26**, 6392 (1987).
[22] X. Liu, K. Zhu, M. Zhang, H. Liu, J. Kang. *J. Biochem. Biophys. Methods*, **52**, 189 (2002).
[23] J.B. Charies, N. Dattagupta, D.M. Crothers. *Biochemistry*, **21**, 3933 (1982).
[24] S. Satyanarayana, J.C. Daborusak, J.B. Charies. *Biochemistry*, **32**, 2573 (1983).
[25] A.K. Patra, M. Nethaji, A.R. Chakravarty. *J. Inorg. Biochem.*, **101**, 233 (2007).
[26] N.M Aghatabay, Y. Mahmiani, H. Cevik, B. Dulger. *Eur. J. Med. Chem.*, **44**, 365 (2009).
[27] M.C.R. Arguelles, P.T. Touceda, R. Cao, A.M.G. Deibe, P. Pelagatti, C. Pelizzi, F. Zani. *J. Inorg. Biochem.*, **103**, 35 (2009).
[28] K. Nakamoto. *Infrared and Raman Spectra of Inorganic and Coordination Compounds*, 5th Edn, J. Wiley, New York (1997).
[29] D.C. Goodman, R.M. Buonomo, P.J. Farmer, J.H. Reibenspie, M.Y. Darensbourg. *Inorg. Chem.*, **35**, 4029 (1996).

[30] A.B.P. Lever. *Inorganic Electronic Spectroscopy*, 2nd Edn, Elsevier, New York (1968).
[31] M.B.H. Howlader, M.S. Islam. *Indian J. Chem.*, **46A**, 440 (2007).
[32] N. Raman, A. Kulandaisamy, C. Thangaraja. *Transition Met. Chem.*, **28**, 29 (2003).
[33] V.T. Kasumov, I. Kartal, F. Koksal. *Spectrochim. Acta, Part A*, 56, 841 (2000).
[34] R. Seangprasertkji, T.L. Riechel. *Inorg. Chem.*, **23**, 988 (1984).
[35] M. Valko, R. Boca, R. Klement, J. Kozisek, M. Mazur, P. Pelikan, H. Morris, H. Elias, L. Muller. *Polyhedron*, **16**, 903 (1997).
[36] S. Djebbar-Sid, O. Benali-Baitich, J.P. Deloume. *Polyhedron*, **16**, 2175 (1997).
[37] R.C. Chikate, S.B. Belapure, S.B. Padhye, D.X. West. *Polyhedron*, **24**, 889 (2005).
[38] N. Raman, S.J. Raja, J.D. Raja, J. Joseph. *Russian J. Coord. Chem.*, **33**, 1 (2007).
[39] L.J. Boucher, T.F. Yen. *Inorg. Chem.*, **8**, 689 (1968).
[40] L.N. Ji, X.H. Zou, J.G. Liu. *Coord. Chem. Rev.*, **216**, 513 (2001).
[41] B.C. Baguley, M. Lebret. *Biochemistry*, **23**, 937 (1984).
[42] M.C. Prabahara, H.S. Bhojya Naik. *Biometals*, **21**, 675 (2008).
[43] T.B. Thederahn, M.D. Kuwabara, T.A. Larsen, D.S. Sigman. *J. Am. Chem. Soc.*, **111**, 4941 (1989).
[44] A.U. Khan. *J. Phys. Chem.*, **80**, 2219 (1976).
[45] T.D. Thangadurai, S.K. Ihm. *J. Ind. Eng. Chem.*, **9**, 563 (2003).
[46] Y. Anjaneyula, R.P. Rao. *Synth. React. Inorg. Met.-Org. Chem.*, **16**, 257 (1986).
[47] N. Dharmaraj, P. Viswanathamurthi, K. Natarajan. *Transition Met. Chem.*, **26**, 105 (2001).